Closed-Form Green's Functions in Planar Layered Media for All Ranges and Materials

Aytaç Alparslan, *Student Member, IEEE*, M. I. Aksun, *Senior Member, IEEE*, and Krzysztof A. Michalski, *Fellow, IEEE*

Abstract—An important extension of the two-level discrete complex image method is proposed to eliminate any concerns on and shortcomings of the approximations of the spatial-domain Green's functions in closed form in planar multilayered media. The proposed approach has been devised to account for the possible wave constituents of a dipole in layered media, such as spherical, cylindrical, and lateral waves, with the aim of obtaining accurate closed-form approximations of Green's functions over all distances from the source. This goal has been achieved by judiciously introducing an additional level into the two-level approach to pick up the contributions of lateral waves in the spatial domain. As a result, three different three-level algorithms have been proposed, investigated, and shown that they work properly over all ranges of distances from the source. In addition to the accuracy of the results at all distances, these approaches also proved to be robust and computationally efficient as compared to the previous algorithms, which can be attributed to the fact that the sampling of the spectral-domain Green's functions in the proposed approaches gives proper emphasis to the associated singularities of the wave types in the spectral domain. However, the judicious choices of the sampling paths may not be enough to get accurate results from the approximations unless the approximating functions in the spectral domain can provide similar wave natures in the spatial domain. To address this issue, the proposed algorithms employ two different approximations; the rational function fitting methods to capture the cylindrical waves (surface waves), and exponential fitting methods to capture both spherical and lateral waves. It is shown and numerically verified that a linear combination of exponential functions in the spectral domain represent the lateral waves at the interface of the involved layers.

Index Terms—Closed-form Green's functions, discrete complex images method (DCIM), Green's functions, layered media.

I. INTRODUCTION

THE METHOD of moments (MoM) is one of the most commonly used numerical techniques in computational electromagnetics for the analysis of layered printed circuits, antennas, and very large scale integration (VLSI) interconnects, at least for small and moderate size geometries [1]–[6]. In the application

A. Alparslan is with the Department of Information Technology and Electrical Engineering, Swiss Federal Institute of Technology, Zürich CH-8092, Switzerland (e-mail: aytac@ieee.org).

M. I. Aksun is with the Department of Electrical and Electronics Engineering, Koç University, 034450 Sariyer, Istanbul, Turkey.

K. A. Michalski is with the Electromagnetics and Microwave Laboratory, Department of Electrical Engineering, Texas A&M University, College Station, TX 77843-3128 USA

of the MoM for the solution of mixed-potential integral equation, the vector and scalar potential Green's functions in the spatial domain must be obtained in advance in order to be able to write the governing equations in the form of an integral equation. However, getting the spatial-domain Green's functions from their spectral-domain counterparts, whose expressions are known analytically for planar layered media, requires the implementation of Hankel transforms, generally referred to as Sommerfeld integrals. Unfortunately, the direct computation of Sommerfeld integrals via numerical integration tools is a time consuming and computationally expensive process due to the oscillatory and slowly decaying nature of the integrands [7], [8]. Motivated by this need, there has been a flurry of interest in the development of efficient algorithms to compute the spatial-domain Green's functions fast and accurately in layered media. The work proposed and discussed in detail in this paper is intended to provide such an algorithm that answers the most, if not all, questions and shortcomings of the currently available approaches.

In the literature, there have been mainly two different approaches to improve the efficiency of computation of Sommerfeld integrals, which are: 1) to evaluate them numerically in conjunction with some transform techniques [8]–[10] or 2) to approximate them in closed forms [11]–[27]. As can be seen from the list of references for the latter approach, which is by no means complete, it has attracted significant amount of interest in the computational electromagnetic (EM) community. The first work published on this approach is considered to be the paper by Fang *et al.*, in 1988 [11], where they proposed approximating the spectral-domain Green's functions in terms of complex exponentials, and transforming them into the spatial domain analytically with the help of the Sommerfeld identity. However, there were a couple of issues that rendered the algorithm inefficient and not robust, which were: 1) the inaccuracy of the resulting image representation at intermediate and large distances (beyond a few wavelengths, even less, depending upon the geometry) and 2) the noise sensitivity and instability of the exponential approximation algorithm used in the work, the Prony's method [28]. As a result, they had to use the so-called "relay race" approach, in which complex images were used up to a distance, beyond which the surface-wave pole (SWP) contributions were used only. It is understandable that not being able to predefine the switching distance encouraged researchers to find a single expression over all ranges involved. Subsequently, unified closed-form expressions for the spatial-domain Green's functions were derived for thick microstrip substrates [12], using almost the same procedure as the one in [11], except for the relay-race implementation. The method started with the extraction of the SWPs and quasi-static terms, and then, the rest was approximated in terms of complex

exponential functions via Prony's method. Hence, transformation of the spectral-domain Green's functions into the spatial domain can be approximated analytically in closed forms, facilitated by the known analytical transforms of the spectral-domain representations of SWP contributions, quasi-static terms, and the discrete complex-image terms. Even though the proposed approach had a few problems to be resolved, which were: 1) the geometry specific extraction of the quasi-static terms; 2) the noise sensitivity of Prony's method; and 3) the large amount of samples required for the implementation of Prony's method, it has inspired a good number of new approaches, modifications, and improvements because of its potential in the development of accurate and efficient computer-aided design (CAD) tools. This approach was first extended to cover more general geometries, i.e., microstrip structures with superstrates [13], with almost no improvement on the problems of the original approach. However, with the introduction of the two-level sampling algorithm that has significantly reduced the number of samples required for the exponential approximation [15], in addition to employing a less noise-sensitive method for the exponential approximation, the generalized pencil-of-function method (GPOF) [14], [29], the resulting algorithm in conjunction with the MoM was considered to have strong potential to be a robust and accurate CAD tool for the analysis of most microwave circuits and printed antennas. Moreover, when the cylindrical wave components, i.e., the surface wave contributions, were handled analytically, or when more exponentials were used in the approximation process, the two-level approach using the GPOF was shown to approximate the spatial-domain Green's functions in closed forms over well beyond a few wavelengths from the source [21], [22].

Meanwhile, there have been plenty of work in the literature to obtain accurate and efficient closed-form representations of the spatial-domain Green's functions, among which the most recent approaches use rational function fitting methods to approximate the spatial-domain Green's functions mainly in terms of Hankel functions [19], [20], [23], [25]–[27]. Although the algorithms based on the rational function fitting initially suffered from inaccuracies in the near-field region due to the singular nature of the approximating Hankel functions as $\rho \to 0$, it has been quickly remedied by: 1) approximating spectral-domain Green's functions as the sum of an asymptotic term and a rational function, whose coefficients are cleverly defined to eliminate the artificial singularities at $\rho \to 0$ in the spatial domain [25] or 2) using a combination of the discrete complex image method (DCIM) and rational function fitting to approximate the spatial-domain Green's function by a sum of spherical waves and cylindrical waves in the near- and far-field regions, respectively [26]. However, as they seem to provide accurate results over all ranges, it was recognized that the far-field results in the vicinity of interfaces for some configurations were not accurate. This was rightfully attributed to the lack of lateral wave contributions in the closed-form representations using cylindrical waves in the far-field region, and has been fixed by adding a new term to the closed-form representation obtained by properly accounting for the new term [27]. Even though these approaches provide accurate results, they may require some sort of tailoring for the specific problems at hand and are quite laborious to implement in conjunction with a MoM-based simulation algorithm.

As one of the contributions of this paper, it is mathematically shown that a combination of spherical waves can mimic the far-field behavior of the lateral waves at the interface of layered media, and therefore, a DCIM-based algorithm can be devised to provide a fully automated, easily implementable, robust, accurate, and efficient alternative to the available methods. Development of such an algorithm is achieved by considering the wave constituents of a dipole in planar layered media, provided the structure is either backed by a perfect electric conductor (PEC) or has identical semiinfinite materials at their outmost layers. This requirement on the geometry is due to the fact that the algorithm developed and presented in this work is designed only for structures supporting a single lateral wave constituent, which corresponds to a single pair of branch points and associated cuts in the spectral-domain representations of the fields in the structure.

Since the proposed algorithm is, in principle, the extension of the two-level approach, with judicious choices of the sampling paths, this paper starts with a brief overview of the two-level DCIM and its known problems in Section II. It is followed, in Section III, by the introduction of three different extensions of the two-level DCIM approximation, resulting in three successful approaches of the three-level DCIM, and demonstrating the robustness of the approach for different choices of paths as long as the wave constituents in the spectral domain are properly sampled and represented. Section IV provides some numerical examples to validate the robustness, accuracy, and ease of implementation of the algorithm for a variety of geometries, and some conclusions are drawn in Section V.

II. SPATIAL-DOMAIN GREEN'S FUNCTIONS AND OVERVIEW OF THE TWO-LEVEL DCIM

A. Spatial-Domain Green's Functions

Transformation of Green's functions from the spectral domain to spatial domain is obtained by the following Sommerfeld integrals:

$$G(\rho) = \frac{1}{4\pi} \int_{\text{SIP}} dk_\rho k_\rho H_0^{(2)}(k_\rho \rho) \tilde{G}(k_\rho) \qquad (1)$$

where $H_0^{(2)}$ is the Hankel function of the second kind, $\tilde{G}$ is the spectral-domain Green's function, which can be obtained analytically for planar multilayered media [14], [30], as seen in Fig. 1, and the Sommerfeld integration path (SIP) is defined in Fig. 2.

Since the whole idea of getting closed-form approximations for the spatial-domain Green's functions originates from the possibility of finding a closed-form approximation of the Sommerfeld integrals (1), one needs to study the integrand carefully for the possible singularities and regions where the contributions to wave constituents are dominant. Although the singularities in the spectral domain—SWPs, branch points, and cuts—and their contributions in the spatial domain—cylindrical and lateral waves—have been well studied and documented [7], [31], it is instructive to summarize some of the facts to help elucidate the implementation of the algorithm in planar layered media composed of left-handed materials (LHMs) and right-handed materials (RHMs). To provide a general picture of the singularities,
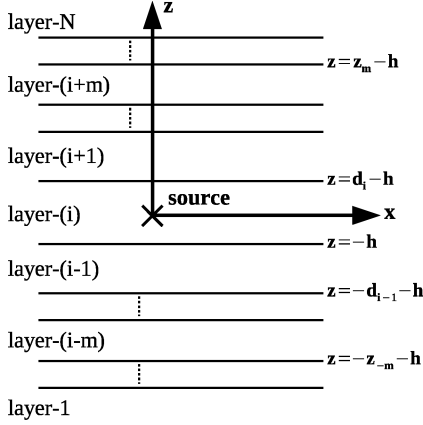
Fig. 1. General multilayered medium. In this work, either layer-1 and layer-N are identical, or one of them is PEC.
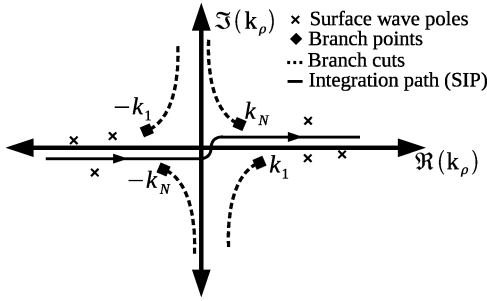

Fig. 2. SIP and possible singularities on the complex k_ρ plane. In this work, there is only one pair of branch points and associated cuts, consistent with the geometrical requirement in the caption of Fig. 1.

layer-1 and layer-N in Fig. 1 are assumed to be lossy RHM and LHM, respectively, and are of semiinfinite extent, thus contributing the branch points at $\pm k_1$ and $\pm k_N$, as shown in Fig. 2 along with the associated branch cuts, for $e^{j\omega t}$ time convention. Regarding the locations of SWPs (surface wave and surface plasmon polariton singularities) for general multilayered structures composed of LHMs, metals (at optical frequencies) and RHMs, they may be found at any location on the k_ρ plane as negative pairs [32]–[35], as opposed to the SWPs in the second and fourth quadrants for the conventional structures of RHMs and perfect conductors.

Once the integration path and possible singularities in the complex k_ρ plane have been defined, in addition to the definition of the Sommerfeld integrals in (1), it can easily be deduced that the integrands of Sommerfeld integrals over the path of integration (SIP or any legitimately deformed path) are quite oscillatory for large distances, and slow convergent in general, rendering numerical integrations time consuming [8]. To overcome this burden, several approaches to approximate the integral in closed form, without referring to commonly employed numerical integration algorithms, have been successfully developed, though with a limited range of distances. Since the goal of this paper is to provide a robust approach, based on DCIM, that would approximate the Sommerfeld integrals in closed forms over all ranges of distances, it is instructive to give a brief overview of the original two-level DCIM [15].

B. Overview of Two-Level DCIM

The idea of DCIM originates from the fact that if the spectral-domain Green's function in (1) can be approximated in terms of exponentials, the Sommerfeld integral (1) can be evaluated analytically by using the well-known Sommerfeld identity

$$\frac{e^{-jkr}}{r} = -\frac{j}{2} \int_{\text{SIP}} dk_\rho k_\rho H_0^{(2)}(k_\rho \rho) \frac{e^{-jk_z|z|}}{k_z} \qquad (2)$$

where $k_z = \sqrt{k^2 - k_\rho^2}$ is the wave vector in the z-direction, r is the spherical radius, and the left-hand expression represents a spherical wave in the spatial domain. In essence, the method facilitates a spherical wave representation of the spatial-domain Green's functions, which usually have other wave components like cylindrical and lateral waves. In the original two-level DCIM [15], the other wave components were not accounted for explicitly because the main goal was to get a simple closed-form expression for the spatial-domain Green's functions in order for them to be easily employed in the MoM implementations. Since it was well known how to handle the SWP contributions explicitly, the most of the problems attributed to the two-level approach would have been resolved with the explicit handling of the SWPs and their contributions, as stated in [21]. Assuming that SWPs are properly extracted in the spectral domain, resulting in

$$\tilde{G}^{(w/o)\text{sw}}(k_\rho) = \tilde{G}(k_\rho) - \tilde{G}^{\text{sw}}(k_\rho) \qquad (3)$$

where $\tilde{G}^{\text{sw}}(k_\rho)$ is the contribution of the SWPs in the spectral domain, and the remaining function $\tilde{G}^{(w/o)\text{sw}}$ can be approximated by complex exponentials via the GPOF method along the two pieces of the path, as shown in Fig. 3 on the k_{zi} and k_ρ planes. The paths are parameterized by

$$\text{For } C_{\text{ap1}}: \quad k_{zi} = -jk_i[T_{02} + t], \qquad 0 \le t \le T_{01}$$
$$\text{For } C_{\text{ap2}}: \quad k_{zi} = k_i\left[-jt + \left(1 - \frac{t}{T_{02}}\right)\right], \qquad 0 \le t \le T_{02} \qquad (4)$$

where t is the real running parameter of the sampling algorithm along the paths, and the limits in the k_ρ-plane, corresponding to the pieces of the path, can be obtained as follows:

$$k_{\rho\max 1} = k_i\sqrt{1 + (T_{01} + T_{02})^2}$$
$$k_{\rho\max 2} = k_i\sqrt{1 + (T_{02})^2} \qquad (5)$$

where k_i and k_{zi} are the wavenumber and the z component of the propagation constant, both in the source layer (layer-i according to Fig. 1), respectively. In the parameterization of the path, T_{02} needs to be chosen so that $k_{\rho\max 2}$ becomes slightly greater than the maximum wavenumber in the structure $k_{\max}$, as shown in Fig. 3(b). Once (3) is sampled along the path and approximated by complex exponentials as

$$\tilde{G}^{(w/o)\text{sw}}(k_\rho) \times jk_{zi} \approx \sum_{l=1}^{2} \sum_{i=1}^{N_l} a_{li} e^{-\alpha_{li} k_{zi}} \qquad (6)$$
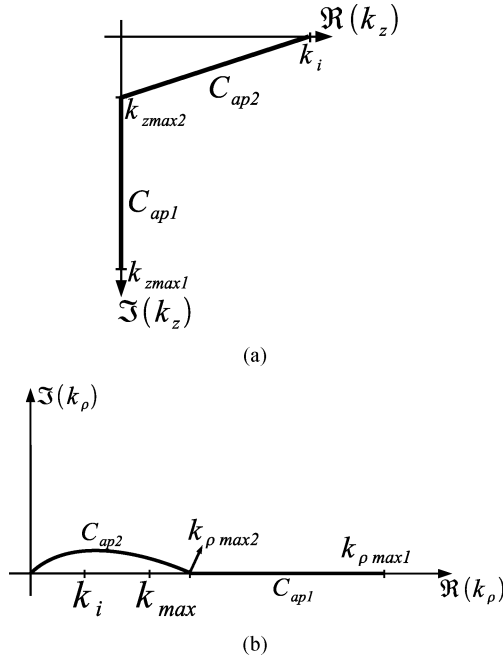
Fig. 3. Paths of approximation for two-level DCIM on the complex: (a) k_{zi} plane and (b) k_ρ plane.

where N_l is the number of exponentials used at each level l, the spatial-domain Green's functions can be written, via the Sommerfeld identity (2), as

$$G(\rho) = G^{\text{sw}}(\rho) + G^{(w/o)\text{sw}}(\rho)$$
$$= G^{\text{sw}}(\rho) + \frac{1}{2\pi} \sum_{l=1}^{2} \sum_{i=1}^{N_l} a_{li} \frac{e^{-jk_i r_{ln}}}{r_{ln}} \qquad (7)$$

where r_{ln} is the distance defined by

$$r_{ln} = \sqrt{\rho^2 + (-j\alpha_{ln})^2} \qquad (8)$$

which is complex in general, and its branch must be chosen so that exponential functions given in (7) decay for large arguments.

The two-level DCIM, as briefly outlined above, has been quite successful in casting the spatial-domain Green's functions in closed forms for most geometries [21], especially when used in the analysis of geometries involved in microwave circuits and printed antennas [6], [36]. However, as pointed out and discussed in [27], its lack of capturing the contribution of the branch point (lateral waves) seems to be an important shortcoming of the method, though only for geometries that support dominant lateral waves in the far field. In general, the contribution of the surface waves dominate in the far field, as surface waves have the following asymptotic behavior for large ρ:

$$\frac{e^{-jk_{\rho p}\rho}}{\sqrt{\rho}} \qquad (9)$$

where $k_{\rho p}$ is the SWP, whereas lateral waves at an interface of two materials behave asymptotically like [7], [31],

$$\frac{e^{-jk_{br}\rho}}{\rho^2} \qquad (10)$$

where k_{br} is the branch point, which is usually a real quantity, as the uppermost and/or lowermost layers are lossless in most of the practical applications. A simple comparison of (9) and (10) reveals that when an SWP has an imaginary part, as in the cases of lossy materials, its contribution decays exponentially, and as a result, the contribution of a branch point, i.e., the lateral wave, determines the far-field behavior of the spatial-domain Green's function. Also for lossless materials, in cases of no proper SWPs or a SWP close to a branch point, the two-level DCIM may result in erroneous data in the far-field region [27]. It is the intention of this paper to propose an algorithm that would provide closed-form spatial-domain Green's functions accurate at all ranges of distances, and carries all the advantages of the DCIM method, such as, simplicity, robustness, and ease of implementation. This goal has been achieved by modifying the path of the two-level approach with a view to incorporate all the wave constituents of a dipole in multilayer planar environment, as discussed in Section III.

III. PROPOSED APPROACH: THREE-LEVEL DCIM

As noted earlier, the two-level approach, together with the explicit handling of the SWPs, is capable of approximating spherical and cylindrical wave constituents, but not the lateral waves, which are due to the branch points in the spectral domain. Therefore, the main modification applied to two-level DCIM has to overcome this shortcoming, i.e., the modification should provide better sampling of the spectral-domain Green's functions around the branch point, in order to capture the wave nature of the lateral wave in the spatial domain. To achieve this, the path $C_{\text{ap}2}$, shown in Fig. 3(b), can be split into two paths by using many different parameterizations, each of which results in a three-level algorithm, and only three of which will be introduced in this section. Note that, in the implementation of the three-level algorithms, SWPs are subtracted *a priori* from the spectral-domain Green's function and handled separately, and that the free-space wavenumber k_0 is assumed to be the only branch point and the minimum wave vector of the structure.

A. Paths for Three-Level DCIM

1) Approach 1: Some modifications on the DCIM path have already been proposed in [22] and [24], where the two pieces of the path for the two-level DCIM were slightly deformed to better capture the SWP contributions when they were not extracted and handled explicitly. However, in the approaches provided here, all the wave constituents are being approximated by suitable functions after their spectral-domain features have been sampled along a path emphasizing these features. Although there are infinitely many variations of the paths, deformed from the path of the two-level DCIM, the first one is a three-level variant of the path given in [24], as shown in Fig. 4(a) and (b) in the k_z and k_ρ planes, respectively, and is parameterized as

For $C_{\text{ap}1}$: $k_{z0} = -jk_0 \left[T_{02} + \frac{T_{01} - T_{02}}{T_{01}} t \right], \qquad 0 \le t \le T_{01}$

For $C_{\text{ap}2}$: $k_{z0} = k_0 \left[(T'_{03} - jT_{03}) - \frac{T'_{03} + j(T_{02} - T_{03})}{T_{02}} t \right],$
$\qquad 0 \le t \le T_{02}$

For $C_{\text{ap}3}$: $k_{z0} = k_0 \left[1 - \frac{1 - T'_{03} + jT_{03}}{T_{03}} t \right], \qquad 0 \le t \le T_{03}.$

$$(11)$$

Fig. 4. Path for the three-level DCIM approach on the complex: (a) k_z plane and (b) k_ρ plane.
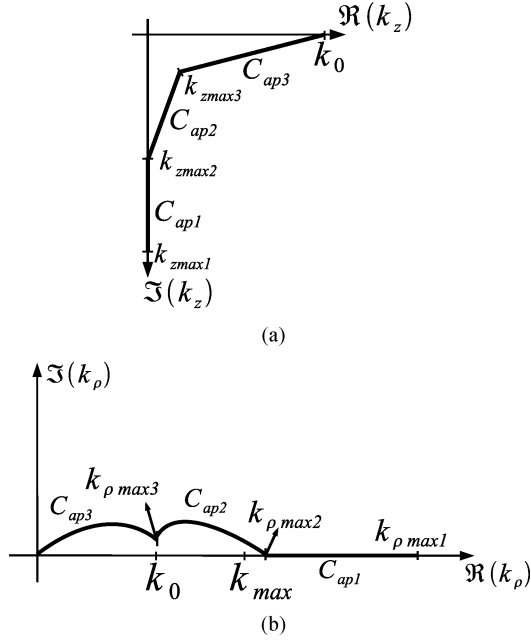

Fig. 5. Path for the three-level DCIM approach on the complex: (a) k_z plane and (b) k_ρ plane.

Note that $k_{\rho \max 1}$, $k_{\rho \max 2}$, and $k_{\rho \max 3}$ in Fig. 4(b) can be easily obtained by $k_\rho = \sqrt{k_0^2 - k_{z0}^2}$, and $k_{\rho \max 2}$ needs to be greater than the maximum wavenumber k_{max} in the structure. As can be observed from Fig. 4(b), the proposed path, deformed from C_{ap2} of the two-level DCIM, was designed to bring the sampling path closer to the branch point k_0 in order to capture the features around the branch point accurately.

2) Approach 2: Another path that would achieve accurate sampling around the branch point is provided in Fig. 5 with the parameterizations of

$$\text{For } C_{\mathrm{ap1}} : k_z = -jk_0 \left[\frac{T_{02}}{T_{03}+1} + t \right], \qquad 0 \leq t \leq T_{01}$$

$$\text{For } C_{\mathrm{ap2}} : k_z = k_0 \left[\frac{1}{T_{03}+1} \right] \left[-jt + \left[1 - \frac{t}{T_{02}} \right] \right],$$
$$0 \leq t \leq T_{02}$$

$$\text{For } C_{\mathrm{ap3}} : k_z = k_0 \left[1 - \frac{t}{T_{03}+1} \right], \qquad 0 \leq t \leq T_{03}. \quad (12)$$

As can be seen from Fig. 5(b), this parameterization eliminates the cusp in the first approach, and provides closer sampling around the branch point. Since the middle piece of the path, C_{ap2}, is almost exclusively over the region where the SWPs are located, one could use the rational function fitting algorithm over this part of the path to extract the SWP contributions numerically, eliminating the need for a robust root-finding algorithm in the method [26]. Note that the extraction of SWPs by using the rational function fitting over the path C_{ap2} must be performed before the implementation of the proposed three-level approximation, and it is only for capturing the surface wave constituents.

3) Approach 3: The third approach for the choice of the path is a simple three-piece real-axis path, motivated by its simplicity
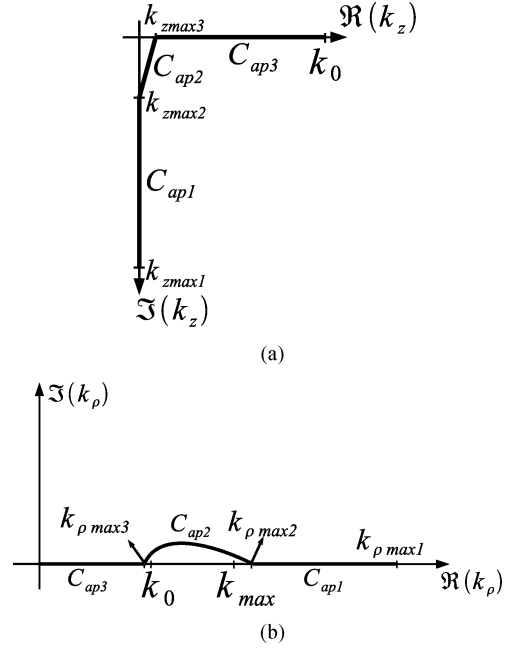
and suitability for structures that contain LHMs and/or metals (at optical frequencies) as well as RHMs, for which SWPs may be anywhere on the k_ρ plane and branch-cuts may extend to infinity in any quadrant on the k_ρ plane, as shown in Fig. 2. Note that the first two approaches are not suitable for such structures, as they are chosen to indent into quadrants where SWPs and branch-cuts cannot be crossed for RHMs with $e^{j\omega t}$ time dependence. Since the path is simply along the real axis of the k_ρ plane, its views on the k_z and k_ρ planes are simple and can be visualized without any graphical aid; hence, only its parametrization is provided as

$$\text{For } C_{\mathrm{ap1}} : k_z = -jk_0[t + T_{02}], \qquad 0 \leq t \leq T_{01}$$
$$\text{For } C_{\mathrm{ap2}} : k_z = -jk_0[t], \qquad 0 \leq t \leq T_{02}$$
$$\text{For } C_{\mathrm{ap3}} : k_z = k_0 \left[1 - \frac{t}{T_{03}} \right], \qquad 0 \leq t \leq T_{03}. \quad (13)$$

At this point, the nature of the SWPs of the structures that contain LHM and/or metallic structures need be overviewed. As seen in Fig. 2, the SWPs appear in pairs, negative of each other, on the complex k_ρ plane: one of them being physical (with a negative imaginary part) and the other being nonphysical (with a positive imaginary part). In the process of subtracting the surface wave contributions from the spectral-domain Green's functions, the SWPs in the first and fourth quadrants of the complex k_ρ plane are taken into account, to obtain a smooth function in the sampling range. However, in adding their contributions to the spatial-domain Green's functions, the physical SWPs, which are on the third and fourth quadrants of the complex k_ρ plane, must be used [37]–[39]. In case of a SWP in the first quadrant of the k_ρ plane, it is subtracted from the spectral-domain Green's function, and its negative pair in the third quadrant is used to

obtain its contribution in the spatial domain, resulting in a backward surface wave [32]–[35]. This behavior cannot be seen in multilayered structures that contain RHMs only, therefore, the sampling paths of two-level DCIM and the first two approaches of the three-level DCIM can be safely used for layered structures that contain only RHMs.

B. Implementation of the Three-Level DCIM

Note that, in all implementations presented here, SWPs are assumed to have been extracted in advance, and the method is applied to the remaining function $\tilde{G}^{(w/o)\text{sw}}(k_\rho)$ given in (3). As the first step of the method, $\tilde{G}^{(w/o)\text{sw}}(k_\rho)$ is sampled along the path C_{ap1}, and approximated by a sum of complex exponentials using the GPOF method, resulting in

$$f_1(k_\rho) \left(= \tilde{G}^{(w/o)\text{sw}}(k_\rho) \times jk_{z0}; k_\rho \in C_{\text{ap1}}\right)$$
$$\cong \sum_{n=1}^{N_1} b_{1n} e^{\beta_{1n} t} = \sum_{n=1}^{N_1} a_{1n} e^{-\alpha_{1n} k_{z0}} \quad (14)$$

where b_{1n} and β_{1n} are the coefficients and exponents obtained from the GPOF method and N_1 is the number of exponentials employed in the first level of the approximation. In addition, the coefficients and exponents transformed into the k_z domain, using corresponding parameterizations of the sampling path, are given by the following.

For approach 1:
$$\alpha_{1n} = \frac{\beta_{1n} T_{01}}{jk_0(T_{01} - T_{02})} \quad a_{1n} = b_{1n} e^{-jk_0 \alpha_{1n} T_{02}}.$$
For approach 2:
$$\alpha_{1n} = \frac{\beta_{1n}}{jk_0} \quad a_{1n} = b_{1n} e^{-jk_0 \alpha_{1n} \frac{T_{02}}{T_{03}+1}}.$$
For approach 3:
$$\alpha_{1n} = \frac{\beta_{1n}}{jk_0} \quad a_{1n} = b_{1n} e^{-jk_0 \alpha_{1n} T_{02}}. \quad (15)$$

After having obtained the first set of exponentials along the path C_{ap1}, they are subtracted from $\tilde{G}^{(w/o)\text{sw}}(k_\rho)$, and the remaining function is sampled along the path C_{ap2} and approximated by the complex exponentials via the GPOF method resulting in

$$f_2(k_\rho)(= \tilde{G}^{(w/o)\text{sw}} \times jk_{z0} - f_1(k_\rho); k_\rho \in C_{\text{ap2}})$$
$$\cong \sum_{n=1}^{N_2} b_{2n} e^{\beta_{2n} t} = \sum_{n=1}^{N_2} a_{2n} e^{-\alpha_{2n} k_{z0}} \quad (16)$$

where b_{2n} and β_{2n} are the coefficients and exponents obtained from the GPOF method, N_2 is the number of exponentials used for the second level of the approximation, and the coefficients and exponents transformed into the k_z domain are given by the following.

For approach 1:
$$\alpha_{2n} = \frac{\beta_{2n} T_{02}}{k_0(j(T_{02} - T_{03}) + T'_{03})}$$
$$a_{2n} = b_{2n} e^{k_0 \alpha_{2n}(T'_{03} - jT_{03})}.$$

For approach 2:
$$\alpha_{2n} = \frac{\beta_{2n} T_{02}(T_{03} + 1)}{k_0(1 + jT_{02})} \quad a_{2n} = b_{2n} e^{k_0 \frac{\alpha_{2n}}{T_{03}+1}}.$$
For approach 3:
$$\alpha_{2n} = \frac{\beta_{2n}}{jk_0} \quad a_{2n} = b_{2n}. \quad (17)$$

The same steps are repeated one more time for the the sampled data collected over the path C_{ap3}, resulting in

$$f_3(k_\rho)(= \tilde{G}^{(w/o)\text{sw}} \times jk_{z0} - f_1(k_\rho) - f_2(k_\rho); k_\rho \in C_{\text{ap3}})$$
$$\cong \sum_{n=1}^{N_3} b_{3n} e^{\beta_{3n} t} = \sum_{n=1}^{N_3} a_{3n} e^{-\alpha_{3n} k_{z0}} \quad (18)$$

where b_{3n} and β_{3n} are the coefficients and exponents obtained from the GPOF method, N_3 is the number of exponentials used for the third level of the approximation, and the coefficients and exponents transformed into the k_z domain are given by the following.

For approach 1:
$$\alpha_{3n} = \frac{\beta_{3n} T_{03}}{k_0(1 - T'_{03} + jT_{03})} \quad a_{3n} = b_{3n} e^{k_0 \alpha_{3n}}.$$
For approach 2:
$$\alpha_{3n} = \frac{\beta_{3n}(T_{03} + 1)}{k_0} \quad a_{3n} = b_{3n} e^{k_0 \alpha_{3n}}.$$
For approach 3:
$$\alpha_{3n} = \frac{\beta_{3n} T_{03}}{k_0} \quad a_{3n} = b_{3n} e^{k_0 \alpha_{3n}}. \quad (19)$$

As the result, combining all the approximating exponentials, in addition to the SWP contributions, the spatial-domain Green's function can be written in closed form as

$$G(\rho) = G^{\text{sw}}(\rho) + G^{(w/o)\text{sw}}(\rho)$$
$$= G^{\text{sw}}(\rho) + \frac{1}{2\pi} \sum_{l=1}^{3} \sum_{i=1}^{N_l} a_{li} \frac{e^{-jk_0 r_{ln}}}{r_{ln}} \quad (20)$$

where r_{ln}'s are defined in (8), the coefficients a_{li} and the exponents α_{li} are defined in (15), (17), and (19) for all three approaches.

C. Capturing the Branch Point Contribution by the Three-Level DCIM

As stated above, the intention of the proposed three-level DCIM approaches is to capture the branch point contribution of a dipole in multilayered planar environments, thus to develop a robust, accurate, and efficient algorithm for the closed-form representation of the spatial-domain Green's functions in such structures. As it is already well known, since the DCIM method is based on the exponential approximation of the spectral-domain Green's functions, it only employs spherical waves in the approximation of the spatial-domain Green's functions. Therefore, to achieve the goal, it is important that the branch point contributions, known as lateral waves, can be accurately and efficiently expressed in terms of spherical waves. In other words, the asymptotic behavior of a combination of spherical waves as

$\rho \to \infty$ has to converge to the asymptotic nature of the lateral wave. Although this point is partially validated by the implementation of the method for several geometries where the lateral waves are the dominant wave constituents in the far field, verifying it mathematically, which is the aim of this section, would guarantee the convergence of the method in such cases.

Before providing the steps of the mathematical demonstration, it would be instructive to note that the asymptotic behavior of the lateral wave, as $\rho \to \infty$ at the interface of the semiinfinite layer, can be shown analytically as $1/\rho^2$, while the spherical waves behave as $1/\rho$. Thus, starting with a spherical wave as

$$a_1 \frac{e^{-jkr_1}}{r_1} \qquad (21)$$

where $r_1 = \sqrt{\rho^2 + (-j\alpha_1)^2}$, and a_1 and α_1 are the coefficient and exponent given in (15), (17), and (19) for the approaches proposed in this paper, its limiting expression as $\rho \to \infty$ can be obtained at the interface as

$$a_1 \frac{e^{-jkr_1}}{r_1} \cong a_1 \frac{e^{-jk\rho}e^{jk\frac{\alpha_1^2}{2\rho}}}{\rho\left(1 - \frac{\alpha_1^2}{2\rho^2}\right)} \cong a_1 \frac{e^{-jk\rho}}{\rho} \frac{1 + jk\frac{\alpha_1^2}{2\rho}}{1 - \frac{\alpha_1^2}{2\rho^2}}. \qquad (22)$$

This expression can be further simplified and cast into a series of powers of $1/\rho$ as

$$a_1 \frac{e^{-jkr_1}}{r_1} \cong a_1 \frac{e^{-jk\rho}}{\rho}\left[1 + jk\frac{\alpha_1^2}{2\rho}\right]\left[1 + \frac{\alpha_1^2}{2\rho^2}\right]$$
$$= a_1 \frac{e^{-jk\rho}}{\rho} + a_1 jk\frac{\alpha_1^2}{2\rho^2}e^{-jk\rho} + O\left(\frac{1}{\rho^3}\right) \qquad (23)$$

by making use of the Binomial expansion of $1/(1 - \alpha_1^2/2\rho^2)$ and retaining its first two terms since $|\alpha_1^2/2\rho^2| \ll 1$ as $\rho \to \infty$. As it can be deduced from this truncated series, a sum of two spherical waves may result in cancellation of $1/\rho$ terms, and be dominated by the $1/\rho^2$ term, if there exist a pair of coefficients and exponents that provide the cancellation. To show the existence of such parameters, two spherical waves with different parameters are added for large ρ values using (23)

$$a_1\frac{e^{-jkr_1}}{r_1} + a_2\frac{e^{-jkr_2}}{r_2} \cong (a_1+a_2)\frac{e^{-jk\rho}}{\rho} + \frac{jk}{2}\left(a_1\alpha_1^2 + a_2\alpha_2^2\right)$$
$$\times \frac{e^{-jk\rho}}{\rho^2} + O\left(\frac{1}{\rho^3}\right) \qquad (24)$$

which proves that the terms with $1/\rho$ dependence in spherical waves (23) cancel out while the terms with $1/\rho^2$ do not for the following combinations of the parameters:

$$a_1 + a_2 \cong 0$$
$$\alpha_1 \mp \alpha_2 \ncong 0. \qquad (25)$$

After having shown mathematically that two spherical waves combined may have an asymptotic behavior of $1/\rho^2$ for large values of ρ, it is time to see if the three-level DCIM algorithms proposed here are capable of capturing the branch point contributions. To test this, a lossy slab backed by the PEC, as shown in Fig. 6 [18], for which the lateral wave contribution is dominant at large distances, was used to obtain the closed-form
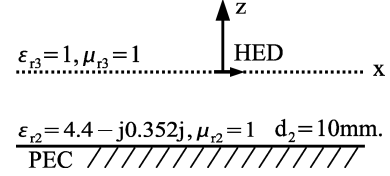

Fig. 6. Geometry that is known to be problematic for the two-level DCIM: a PEC backed, lossy slab [18].

TABLE I
PERFORMANCE OF DCIMS TO CAPTURE LATERAL WAVES†

Method	T_{02}	$T_{03}(-T'_{03})$	$a_1 + a_2$
2-lvl	2	–	$4.99 \times 10^{-3} - j2.61 \times 10^{-1}$
3-lvl - 1	0.1	0.01 − 0.01	$-2.00 \times 10^{-6} - j9.98 \times 10^{-7}$
3-lvl - 1	2	0.01 − 0.01	$-7.92 \times 10^{-3} + j5.43 \times 10^{-4}$
3-lvl - 2	1	99	$2.64 \times 10^{-9} - j1.14 \times 10^{-9}$
3-lvl - 2	200	99	$-6.83 \times 10^{-3} + j3.62 \times 10^{-4}$
3-lvl - 3	0.01	–	$-3.65 \times 10^{-11} + j1.56 \times 10^{-11}$
3-lvl - 3	2	–	$-6.63 \times 10^{-3} + j1.45 \times 10^{-3}$

†The parameters are for the path C_{ap2} only, and 100 samples are used along this path.

expression for $\tilde{G}_{xx}^A$, the x component of the vector-potential Green's function generated by an x-directed dipole. Note that the closed-form Green's function was obtained at the interface, where the source is located, at the operating frequency of $f = 10$ GHz, and before the implementation of the algorithms, the only contributing SWP to $\tilde{G}_{xx}^A$ was found at $k_{\text{sw,TE}} = (1.7418 - j0.0909)k_0$ and subtracted from the spectral-domain Green's function. As a result of the implementations of the three-level DCIMs over the path C_{ap2} to the resulting spectral-domain expression, it can be observed from Table I that a simple combination of two spherical waves with appropriate weights $(a_1 + a_2 \cong 0)$ results in a wave nature of $1/\rho^2$ spatial dependence. As expected, the closer the path goes around the branch point k_0, as it does for the lower values of T_{02}, the better the cancellation of the spherical wave components in all three approaches. Note that the two-level approach cannot capture the contribution of the branch point, as the value of $a_1 + a_2$ is relatively high. Further studies on the performance of the three-level DCIMs, as compared to the two-level DCIM, are given in Section IV.

IV. NUMERICAL EXAMPLES

In this section, several layered structures that belong to the problematic cases of the preexisting DCIM-based and rational-function-fitting-based algorithms, as described in [27], are studied using the three-level approaches presented in Section III, and the resulting Green's functions are provided over an extended range to demonstrate the robustness, efficiency, and accuracy of the algorithms over all ranges. Although the results are shown in the figures up to $k_0\rho = 10^4$, they actually predict the asymptotic behavior of the Green's functions very accurately as $\rho \to \infty$. Note that, for all the cases studied, all components of the Green's functions for the scalar and vector potentials were examined and found to

be in very good agreement with the exact data obtained by the numerical integration of the corresponding Sommerfeld integrals. However, for the sake of brevity, only the plots of the scalar potential G_x^q and the vector potential G_{xx}^A are provided.

A. Geometry With No SWPs, Approach 1

As it is well known, TE and TM surface waves are generally supported in layered structures, and form the discrete spectrum of the Green's functions. However, certain components of the dyadic Green's function for the vector potential, e.g., G_{xx}^A, may have surface wave contributions of TE type only, having a cutoff frequency below which it can not be supported in the structure. Hence, the geometry and frequency of the operation for this example are chosen, as given in [27], such that TE surface wave poles are not supported, and the Green's function for the vector potential G_{xx}^A is studied to see if Approach 1 can predict the asymptotic behavior of the vector potential in the case of dominant lateral waves. Here are the parameters of the structure based on the descriptions in Fig. 1: layer-1 is the PEC; layer-2 is a dielectric slab with $\varepsilon_{r2} = 4.4$ and thickness $d_2 = 10$ mm; layer-3 is semiinfinite free space; the locations of the source [horizontal electric dipole (HED)] and observation points are at the interface between the free space and dielectric layer ($h = z = 0$); and the frequency of operation is $f = 3$ GHz. Note that there is only one TM-mode SWP at $k_{\rho p(\text{TM})} = 1.2247 k_0$ in the structure at the given frequency, whose contribution needs to be accounted for in the computation of the scalar potential Green's function $\tilde{G}_x^q$. The results of the numerical integration and those of the two- and three-level DCIMs are provided in Figs. 7 and 8 for the vector and scalar potential Green's functions, respectively. For the purpose of comparison, here are the parameters of the implementations of DCIMs for this example: for the two-level DCIM, $T_{01} = 100$ and $T_{02} = 2$, number of samples $= 100$ for each path involved, and the number of exponentials used are $N_1 = 4$ and $N_2 = 4$ for the vector potential and $N_1 = 5$ and $N_2 = 4$ for the scalar potential Green's functions; for the three-level DCIM, $T_{01} = 100, T_{02} = 2$, and $T_{03} = T'_{03} = 0.01$, number of samples $= 100$ for each path involved, and the number of exponentials used are $N_1 = 4, N_2 = 3$, and $N_3 = 4$ for the vector potential and $N_1 = 5, N_2 = 4$, and $N_3 = 4$ for the scalar potential Green's functions.

As discussed earlier, the two-level DCIM cannot capture the branch point contribution in the vector potential Green's function, and consequently results in the far-field behavior of $1/\rho$ dependence, introducing errors for $\rho \to \infty$, as shown in Fig. 7. On the other hand, Approach 1 of the three-level DCIM captures the branch point contribution, and results in an excellent agreement with the data obtained by the numerical integration, not only in the near- and intermediate-field regions, but also in the far-field zone. In the case of scalar potential Green's functions, since the surface wave contribution dominates the far-field behavior of the potential, regardless of the performance of the methods for capturing the branch point contribution, both two- and three-level DCIM algorithms work fine, as shown in Fig. 8. Note that all three approaches based on the three-level DCIM algorithm work very well for all the examples studied, but for the structures with LHMs, the paths defined in Approach 3 are
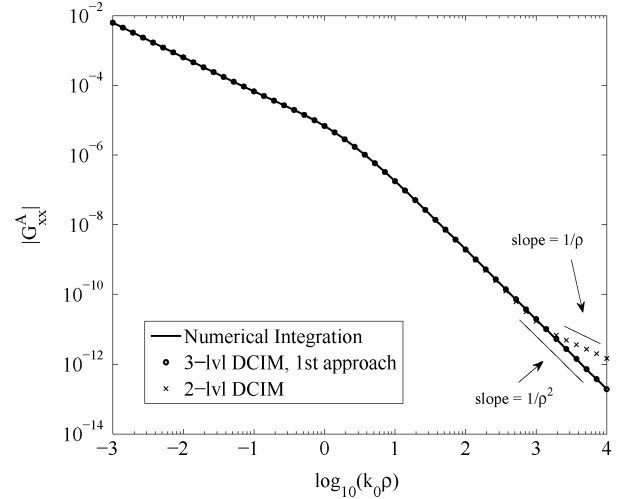

Fig. 7. Magnitude of vector potential Green's function for the three-layer geometry with the following parameters: layer-1: PEC; layer-2: $\varepsilon_{r2} = 4.4, \mu_{r2} = 1, d_2 = 10$ mm; layer-3: free space; $f = 3$ GHz; $h = z = 0$.
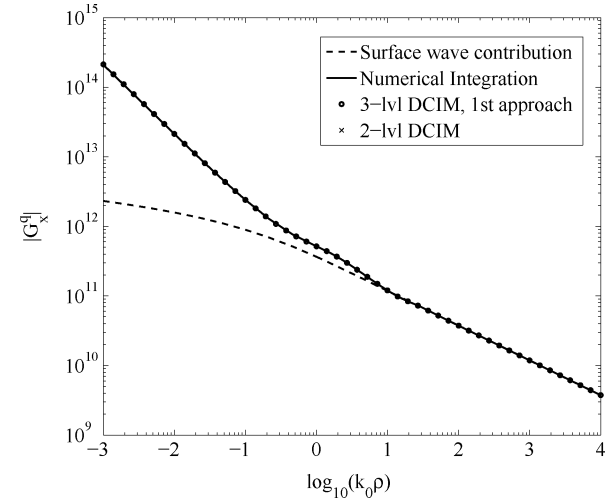

Fig. 8. Magnitude of scalar potential Green's function for the three-layer geometry with the following parameters: layer-1: PEC; layer-2: $\varepsilon_{r2} = 4.4, \mu_{r2} = 1, d_2 = 10$ mm; layer-3: free space; $f = 3$ GHz; $h = z = 0$.

employed only, in order to avoid crossing the branch-cuts and surface wave poles involved.

B. Geometry With Lossy Layer, Approach 2

To provide a similar example for the implementation of Approach 2, the structure given in [18] was used with the following parameters: layer-1 is PEC; layer-2 is a lossy dielectric slab with $\varepsilon_{r2} = 4.4 - j0.352$ and thickness $d_2 = 10$ mm; layer-3 is semiinfinite free space; the locations of the source (HED) and observation points are at the interface between the free space and the dielectric layer ($h = z = 0$); and the frequency of operation is $f = 10$ GHz. Note that, for this configuration, there are two TM-mode SWPs at $k_{\rho p(\text{TM})(1)} = (1.0451 - j0.0298)k_0$, and $k_{\rho p(\text{TM})(2)} = (1.9772 - j0.0870)k_0$, and one TE-mode SWP at $k_{\rho p(\text{TE})} = (1.7418 - j0.0909)k_0$.

The difference of this example from the previous one is that both potentials have surface wave constituents, but due to the
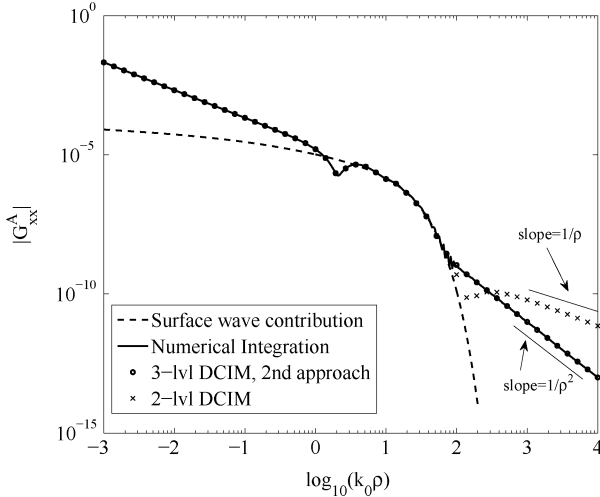
Fig. 9. Magnitude of vector potential Green's function for the three-layer structure with the following parameters: layer-1: PEC; layer-2: $\varepsilon_{r2} = 4.4 - j0.352, \mu_{r2} = 1, d_2 = 10$ mm; layer-3: free space; $f = 10$ GHz; $h = z = 0$.
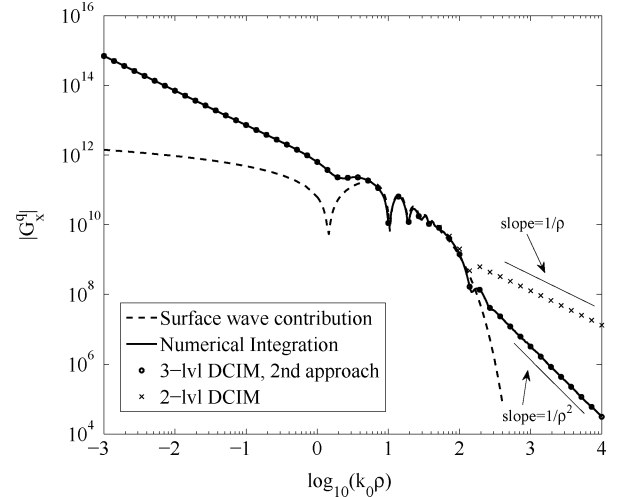

Fig. 10. Magnitude of scalar potential Green's function for the three-layer structure with the following parameters: layer-1: PEC; layer-2: $\varepsilon_{r2} = 4.4 - j0.352, \mu_{r2} = 1, d_2 = 10$ mm; layer-3: free space; $f = 10$ GHz; $h = z = 0$.

loss in the medium, surface waves are expected to decay exponentially as $\rho \to \infty$, resulting in dominant lateral wave constituents in this region, as seen in Figs. 9 and 10. Note that the surface wave components of the potentials were provided in all figures in order to see the comparative nature of the wave constituents of a dipole source in layered media. In order to assess the performance of Approach 2 in a structure where the dominating asymptotic behavior of the waves is $1/\rho^2$, the vector and scalar potential Green's functions were obtained in closed form and compared to the results of the numerical integration and the two-level DCIM, as shown in Figs. 9 and 10, respectively. Similar to the previous example, while the two-level DCIM is not able to capture the branch-point contribution, Approach 2 of the three-level DCIM algorithms predicts the distribution of the potentials very well, not only in the range where the lateral wave is the dominant wave constituent, but over the entire range, with the correct asymptotic behavior as $\rho \to \infty$, as seen in Figs. 9 and 10. Here are the parameters of the implementations of DCIMs for this example: for the two-level DCIM, $T_{01} = 100$ and $T_{02} = 2$, number of samples = 100 for each path involved, and the number of exponentials used are $N_1 = 5$ and $N_2 = 4$ for the vector potential, and $N_1 = 5$ and $N_2 = 5$ for the scalar potential Green's functions; for the three-level DCIM, $T_{01} = 100, T_{02} = 200$, and $T_{03} = 99$, number of samples = 100 for each path involved, and the number of exponentials used are $N_1 = 4, N_2 = 4$, and $N_3 = 4$ for the vector potential and $N_1 = 4, N_2 = 4$, and $N_3 = 5$ for the scalar potential Green's functions.

C. A Geometry With Lossy LHM, Approach 3

As discussed in Section II, SWPs can be found anywhere in the complex k_ρ-plane for layered structures consisting of LHMs and/or metals (in optic frequencies) in addition to RHMs. Therefore, the paths of Approach 1 and Approach 2 of the three-level DCIM algorithms may not be suitable, as they may cross the branch-cuts or singularities in the process of deformation from SIP. To eliminate this possibility for such configurations, the

approximation paths of Approach 3 were so defined as to stay on the real k_ρ axis, as detailed in Section III. This example is chosen to cover this special case and to demonstrate the robustness and efficiency of the three-level DCIM for planar layered structures composed of arbitrary materials. Here are the details of the structure, as referenced to Fig. 1: layer-1 is PEC; layer-2 is a lossy homogeneous LHM slab with $\varepsilon_{r2} = -2 - j0.01, \mu_{r2} = -1.5 - j0.01$ and thickness $d_2 = 15.5$ cm; layer-3 is free space; source (HED) and observation points are chosen at the interface between the free space and the dielectric layer ($h = z = 0$); and the frequency of operation is $f = 1$ GHz. For this configuration, there are total of three SWPs; one TM-mode at $k_{\rho\rho(\text{TM})} = (-1.6432 - j0.0110)k_0$ and two TE-mode at $k_{\rho\rho(\text{TE})(1)} = (1.0070 - j0.0068)k_0$ and $k_{\rho\rho(\text{TE})(2)} = (-1.2121 - j0.0286)k_0$. At this point it must be noted again that the SWPs with $\Re(k_{\rho\rho}) > 0$ are subtracted from the spectral-domain Green's function before the GPOF method is applied (for this example, SWPs at $-k_{\rho\rho(\text{TM})}, k_{\rho\rho(\text{TE})(1)}$ and $-k_{\rho\rho(\text{TE})(2)}$ are subtracted), and their contributions are added to the spatial-domain Green's functions by using the physical ones, i.e., SWPs with negative imaginary parts, (for this example, SWPs at $k_{\rho\rho(\text{TM})}, k_{\rho\rho(\text{TE})(1)}$ and $k_{\rho\rho(\text{TE})(2)}$ are added).

After having implemented Approach 3 for this configuration, the closed-form Green's functions and their explicit surface wave constituents were obtained and compared to the result obtained by the numerical integration of the corresponding Sommerfeld integrals, as shown in Figs. 11 and 12 for vector and scalar potentials, respectively. It is obvious that the results obtained by the three-level DCIM and by the numerical integration agree extremely well, even though the asymptotic trend is not dominated by the surface waves. It should be noted that this observation is not limited to this specific example, but is valid for all the cases studied during this work, the list of which may not be exhaustive, but definitely covers a broad spectrum of layered structures. For the sake of completeness, the parameters used in the implementation of the three-level DCIM, approach 3, are given as follows: $T_{01} = 100$ and $T_{02} = 2(k_0\sqrt{1 + T_{02}^2} >$
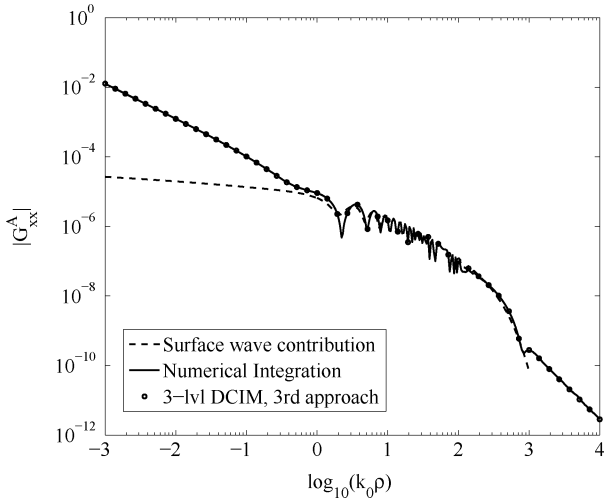
Fig. 11. Magnitude of vector potential Green's function for the three-layer structure with the following parameters: layer-1: PEC; layer-2: LHM with $\varepsilon_{r2} = -2 - j0.01, \mu_{r2} = -1.5 - j0.01, d_2 = 15.5$ cm; layer-3: free space; $f = 1$ GHz; $h = z = 0$.
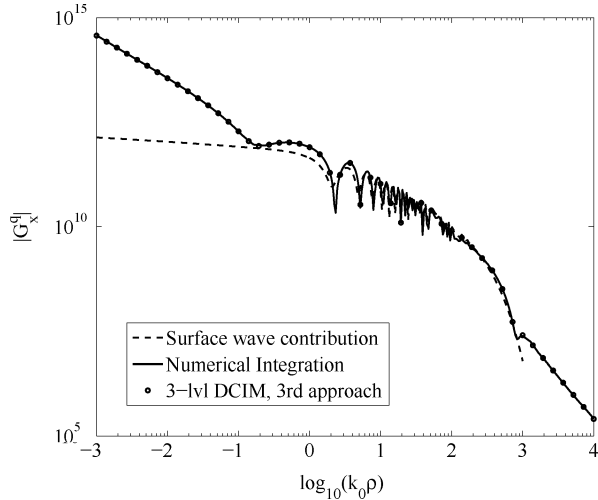

Fig. 12. Magnitude of scalar potential Green's function for the three-layer structure with the following parameters: layer-1: PEC; layer-2: LHM with $\varepsilon_{r2} = -2 - j0.01, \mu_{r2} = -1.5 - j0.01, d_2 = 15.5$ cm; layer-3: free space; $f = 1$ GHz; $h = z = 0$.

$|\Re(k_0 \sqrt{(-2 - j0.01)(-1.5 - j0.01)})|)$, number of samples $= 100$ for each path involved, and the number of exponentials used are $N_1 = 4, N_2 = 6$, and $N_3 = 6$ for the vector potential, and $N_1 = 4, N_2 = 6$, and $N_3 = 6$ for the scalar potential Green's functions.

D. A Multilayered Geometry for Plasmonic Applications

Once the proposed approaches have been tested on the geometries that were introduced as the problematic cases of the DCIM in the literature, Green's functions of a general multilayered structure, consisting of lossless and lossy dielectric materials and metals, are obtained at optical wavelengths by using the proposed approaches. The main motivation for such an example is to demonstrate the true potential of the proposed approach by examining a rather complex and popular structure (due to the recent popularity of plasmonics) in optical regime.
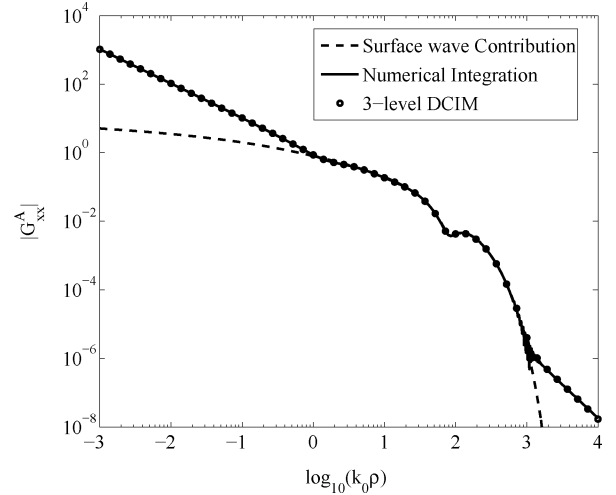

Fig. 13. Magnitude of vector potential Green's function for the five-layer plasmonic structure with the following parameters: layer-1: free-space; layer-2: a lossless dielectric material with $\varepsilon_{r2} = 2.0, \mu_{r2} = 1.0, d_2 = 200$ nm; layer-3: gold with $\varepsilon_{r3} = -9.31 - j1.53, \mu_{r3} = 1.0, d_3 = 60$ nm; layer-4: a lossy dielectric material with $\varepsilon_{r4} = 2.0 - j0.1, \mu_{r4} = 1.0, d_4 = 200$ nm; layer-5: free space; $\lambda_0 = 600$ nm; HED is at the interface between layer-4 and layer-5, $h = z = 0$.

The details of the operation and the structure, as referenced to Fig. 1, are as follows: layer-1 and layer-5 are free space; layer-2 is a lossless dielectric material with $\varepsilon_{r2} = 2, d_2 = 200$ nm; layer-3 is made out of gold with $\varepsilon_{r3} = -9.31 - j1.53, \mu_{r3} = 1.0, d_3 = 60$ nm, which can support surface plasmon polaritons at the interface; layer-4 is a lossy dielectric material with $\varepsilon_{r4} = 2.0 - j0.1, d_4 = 200$ nm; the operating free-space wavelength is $\lambda_0 = 600$ nm and the source (in this case, HED) and the observation planes are chosen at the interface between layer-4 and layer-5, i.e., $h = z = 0$. Moreover, there are a total of four SWPs supported by this configuration at the operating point: $k_{\rho\rho(\text{TM})(1)} = (1.4959 - j0.0403)k_0, k_{\rho\rho(\text{TM})(2)} = (1.6648 - j0.1023)k_0, k_{\rho\rho(\text{TE})(1)} = (1.1124 - j0.0080)k_0$, and $k_{\rho\rho(\text{TE})(2)} = (1.1172 - j0.0281)k_0$. It would be worth noting that the two of the SWPs (both TM types) were found in the region above the wavenumber of the densest dielectric medium in the structure because of the existence of a thin gold layer in the structure.

For the sake of completeness and assessing the comparative computational advantages of all three approaches proposed in this work, they have been implemented on this structure, resulting in identical spatial-domain Green's functions, as shown in Figs. 13 and 14 for the vector and scalar potentials, respectively. In addition, it is observed that the number of exponentials employed in all approaches, even in each level, are identical, namely, (5, 5, 5) for the vector potential and (5, 6, 5) for the scalar potential corresponding to the approximations over $(C_{\text{ap1}}, C_{\text{ap2}}, C_{\text{ap3}})$. Although adding one more level into the two-level approach adds one more implementation of the GPOF method, the computational complexity of the approach has not been affected significantly because identifying the major contributing regions in the spectral domain and utilizing this information result in a better approximation with a lesser number of exponentials, even for a large number of layers in the structure.
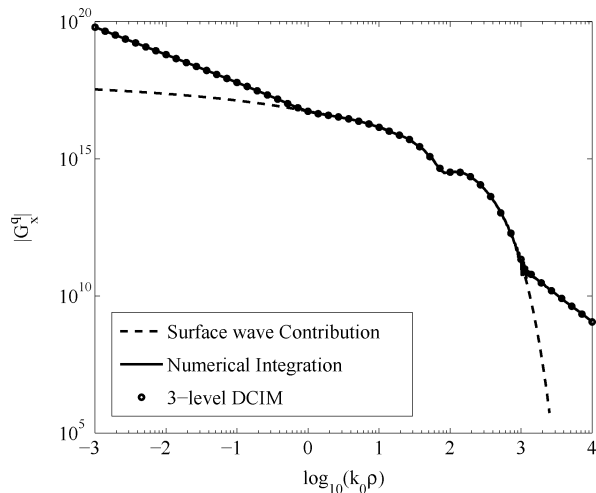
Fig. 14. Magnitude of scalar potential Green's function for the five-layer plasmonic structure with the following parameters: layer-1: free-space; layer-2: lossless dielectric material with $\varepsilon_{r2} = 2.0, \mu_{r2} = 1.0, d_2 = 200$ nm; layer-3: gold with $\varepsilon_{r3} = -9.31 - j1.53, \mu_{r3} = 1.0, d_3 = 60$ nm; layer-4: a lossy dielectric material with $\varepsilon_{r4} = 2.0 - j0.1, \mu_{r4} = 1.0, d_4 = 200$ nm; layer-5: free space; $\lambda_0 = 600$ nm; HED is at the interface between layer-4 and layer-5 $h = z = 0$.

V. CONCLUSION

In this paper, three DCIM-based algorithms have been proposed to obtain the closed-form Green's functions over all ranges in planar layered media, giving proper emphasis to the wave natures of different singularities in the spectral-domain representations. Although the three proposed algorithms are mainly three-level DCIMs, a DCIM with any number of paths, i.e., the level, may be devised and employed, as long as capturing the signature of each singularity in the spectral domain properly. Using the proposed three-level DCIM approaches, the mostly pronounced drawback of the algorithms based on DCIM, i.e., their lack of approximating the lateral wave nature, has been alleviated by introducing an additional path around the branch point into the already available two-level DCIM approach. It has been demonstrated that these approaches work very well and provide very accurate closed-form Green's functions, not only over all ranges of distances from the source, but for any material type, including LHMs. Note that the success of the algorithm proposed here is based on a single assumption; a combination of spherical waves can accurately represent lateral waves. As a part of the contribution in this work, this assumption was verified mathematically, in addition to its numerical verification in many examples, showing that the sum of two complex images, with proper choices of their coefficients and exponents, can accurately mimic the lateral wave behavior in the far-field zone at an interface. Consequently, the proposed algorithm, with its three variants, can be considered robust, efficient, and easy to implement, and therefore, is a viable tool to be employed in a CAD package.

REFERENCES

[1] J. R. Mosig, "Arbitrarily shaped microstrip structures and their analysis with a mixed potential integral equation," *IEEE Trans. Microw. Theory Tech.*, vol. 36, no. 2, pp. 314–323, Feb. 1988.

[2] L. Alatan, M. I. Aksun, K. Mahadevan, and T. Birand, "Analytical evaluation of the MoM matrix elements," *IEEE Trans. Microw. Theory Tech.*, vol. 44, no. 4, pp. 519–525, Apr. 1996.

[3] M. J. Tsai, F. D. Flavis, O. Fordharn, and N. G. Alexopoulos, "Modeling planar arbitrarily shaped microstrip elements in multilayered media," *IEEE Trans. Microw. Theory Tech.*, vol. 45, no. 3, pp. 330–337, Mar. 1997.

[4] M. R. Abdul-Gaffoor, H. K. Smith, A. A. Kishk, and A. W. Glisson, "Simple and efficient full-wave modeling of electromagnetic coupling in realistic RF multilayer PCB layouts," *IEEE Trans. Microw. Theory Tech.*, vol. 50, no. 6, pp. 1445–1457, Jun. 2002.

[5] N. Kinayman and M. I. Aksun, *Modern Microwave Circuits*. Norwood, MA: Artech House, 2005.

[6] T. Onal, M. I. Aksun, and N. Kinayman, "A rigorous and efficient analysis of 3-D printed circuits: Vertical conductors arbitrarily distributed in multilayer environment," *IEEE Trans. Antennas Propag.*, vol. 55, no. 12, pp. 3726–3729, Dec. 2007.

[7] W. C. Chew, *Waves and Fields in Inhomogeneous Media*. New York: Van Nostrand, 1990.

[8] K. A. Michalski, "Extrapolation methods for sommerfeld integral tails," *IEEE Trans. Antennas Propag.*, vol. 46, no. 10, pp. 1405–1418, Oct. 1998.

[9] J. R. Mosig and F. E. Gardiol, "A dynamical radiation model for microstrip structures," in *Advances in Electronics and Electron Physics*, P. W. Hawkes, Ed. New York: Academic, 1982, vol. 59, pp. 139–237.

[10] N. Kinayman and M. I. Aksun, "Comparative study of acceleration techniques for integrals and series in electromagnetic problems," *Radio Sci.*, vol. 30, pp. 1713–1722, Nov.–Dec. 1995.

[11] D. C. Fang, J. J. Yang, and G. Y. Delisle, "Discrete image theory for horizontal electric dipoles in a multilayered medium," *Proc. IEEE*, vol. 135, no. 5, pp. 297–303, May 1988.

[12] Y. L. Chow, J. J. Yang, D. G. Fang, and G. E. Howard, "A closed-form spatial Green's function for the thick microstrip substrate," *IEEE Trans. Microw. Theory Tech.*, vol. 39, no. 3, pp. 588–592, Mar. 1991.

[13] M. I. Aksun and R. Mittra, "Derivation of closed-form Green's functions for a general microstrip geometry," *IEEE Trans. Microw. Theory Tech.*, vol. 40, no. 11, pp. 2055–2062, Nov. 1992.

[14] G. Dural and M. I. Aksun, "Closed-form Green's functions for general sources and stratified media," *IEEE Trans. Microw. Theory Tech.*, vol. 43, no. 7, pp. 1545–1552, Jul. 1995.

[15] M. I. Aksun, "A robust approach for the derivation of closed-form Green's functions," *IEEE Trans. Microw. Theory Tech.*, vol. 44, no. 5, pp. 651–658, May 1996.

[16] C. Tokgoz and G. Dural, "Closed-form Green's functions for cylindrically stratified media," *IEEE Trans. Microw. Theory Tech.*, vol. 48, no. 1, pp. 40–49, Jan. 2000.

[17] Y. Ge and K. P. Esselle, "New closed-form Green's functions for microstrip structures theory and results," *IEEE Trans. Microw. Theory Tech.*, vol. 50, no. 6, pp. 1556–1560, Jun. 2002.

[18] N. V. Shuley, R. R. Boix, F. Medina, and M. Horno, "On the fast approximation of Green's functions in MPIE formulations for planar layered media," *IEEE Trans. Microw. Theory Tech.*, vol. 50, no. 9, pp. 2185–2192, Sep. 2002.

[19] V. I. Okhmatovski and A. C. Cangellaris, "A new technique for the derivation of closed-form electromagnetic Green's functions for unbounded planar layered media," *IEEE Trans. Antennas Propag.*, vol. 50, no. 7, pp. 1005–1016, Jul. 2002.

[20] V. I. Okhmatovski and A. C. Cangellaris, "Evaluation of layered media Green's functions via rational function fitting," *IEEE Microw. Wireless Compon. Lett.*, vol. 14, no. 1, pp. 22–24, Jan. 2004.

[21] M. I. Aksun and G. Dural, "Clarification of issues on the closed-form Green's functions in stratified media," *IEEE Trans. Antennas Propag.*, vol. 53, no. 11, pp. 3644–3653, Nov. 2005.

[22] M. Yuan, T. K. Sarkar, and M. Salazar-Palma, "A direct discrete complex image method from the closed-form Green's functions in multilayered media," *IEEE Trans. Microw. Theory Tech.*, vol. 54, no. 3, pp. 1025–1032, Mar. 2006.

[23] V. N. Kourkoulos and A. C. Cangellaris, "Accurate approximation of Green's functions in planar stratified media in terms of a finite sum of spherical and cylindrical waves," *IEEE Trans. Antennas Propag.*, vol. 54, no. 5, pp. 1568–1576, May 2006.

[24] L. Zhuang, G. Zhu, Y. Zhang, and B. Xiao, "An improved discrete complex image method for Green's functions in multilayered media," *Microw. Opt. Technol. Lett.*, vol. 49, no. 6, pp. 1337–1340, 2007.

[25] R. R. Boix, F. Mesa, and F. Medina, "Application of total least squares to the derivation of closed-form Green's functions for planar layered media," *IEEE Trans. Microw. Theory Tech.*, vol. 55, no. 2, pp. 268–280, Feb. 2007.

[26] A. G. Polimeridis, T. V. Yioultsis, and T. D. Tsiboukis, "A robust method for the computation of Green's functions in stratified media," *IEEE Trans. Antennas Propag.*, vol. 55, no. 7, pp. 1963–1969, Jul. 2007.

[27] F. Mesa, R. R. Boix, and F. Medina, "Closed-form expressions of multilayered planar Green's functions that account for the continuous spectrum in the far field," *IEEE Trans. Microw. Theory Tech.*, vol. 56, no. 7, pp. 1601–1614, Jul. 2008.

[28] R. W. Hamming, *Numerical Methods for Scientists and Engineers*. New York: Dover, 1973.

[29] Y. Hua and T. K. Sarkar, "Generalized pencil-of-function method for extracting poles of an EM system from its transient response," *IEEE Trans. Antennas Propag.*, vol. 37, no. 2, pp. 229–234, Feb. 1989.

[30] K. A. Michalski and J. R. Mosig, "Multilayered media Green's functions in integral equation formulations," *IEEE Trans. Antennas Propag.*, vol. 45, no. 3, pp. 508–519, Mar. 1997.

[31] N. Felsen and L. B. Marcuvitz, *Radiation and Scattering of Waves*. New York: Wiley, 1994.

[32] H. Cory and A. Barger, "Surface-wave propagation along a metamaterial slab," *Microw. Opt. Technol. Lett.*, vol. 38, no. 5, pp. 392–395, Sep. 2003.

[33] B.-I. Wu, T. M. Grzegorczyk, J. Zhang, and J. A. Kong, "Guided modes with imaginary transverse wave number in a slab waveguide with negative permittivity and permeability," *J. Appl. Phys.*, vol. 93, no. 11, pp. 9386–9388, 2003.

[34] J. Lu, M. Grzegorczyk, B.-I. Wu, J. Pacheco, M. Chen, and J. A. Kong, "Effect of poles on subwavelength focusing by an LHM slab," *Microw. Opt. Technol. Lett.*, vol. 45, no. 1, pp. 49–53, Apr. 2005.

[35] P. Baccarelli, P. Burghignoli, F. Frezza, A. Galli, P. Lampariello, G. Lovat, and S. Paulotto, "Fundamental modal properties of surface waves on metamaterial grounded slabs," *IEEE Trans. Microw. Theory Tech.*, vol. 53, no. 4, pp. 1431–1442, Apr. 2005.

[36] T. Onal, M. I. Aksun, and N. Kinayman, "An efficient full-wave simulation algorithm for multiple vertical conductors in printed circuits," *IEEE Trans. Microw. Theory Tech.*, vol. 54, no. 10, pp. 3739–3745, Oct. 2006.

[37] W. C. Chew, "Sommerfeld integrals for left-handed materials," *Microw. Opt. Technol. Lett.*, vol. 42, no. 5, pp. 369–373, 2004.

[38] J. Q. Bagley, B. Wu, and L. Tsang, "Electromagnetic fields of Hertzian dipoles in layered negative refractive index materials," *IEEE Antennas Wireless Propag. Lett.*, vol. 7, pp. 749–752, 2008.

[39] W. Shu and J. Song, "Sommerfeld integration path for double negative metamaterials," in *IEEE AP-S Int. Symp.*, Jul. 2008, pp. 1–4.

Aytaç Alparslan (S'04) received the B.S. and M.S. degrees in electrical and electronic engineering from Koç University, Istanbul, Turkey, in 2006 and 2008, respectively, and is currently working toward the Ph.D. degree in information technology and electrical engineering at ETH Zürich, Zürich, Switzerland.

His research interests include computational electromagnetics, metamaterials and photonic-bandgap structures and nanophotonics.

Mr. Alparslan was the recipient of the Undergraduate Scholarship presented by the IEEE Microwave Theory and Techniques Society (IEEE MTT-S) and the IEEE Antennas and Propagation Society (IEEE AP-S) in 2005. He was also a recipient of the TÜBİTAK Graduate Scholarship in 2006–2008.

M. I. Aksun (M'92–SM'99) received the B.S. and M.S. degrees in electrical and electronics engineering from Middle East Technical University, Ankara, Turkey, in 1981 and 1983, respectively, and the Ph.D. degree in electrical and computer engineering from the University of Illinois at Urbana-Champaign, in 1990.

From 1990 to 1992, he was a Post-Doctoral Fellow with the Electromagnetic Communication Laboratory, University of Illinois at Urbana-Champaign. From 1992 to 2001, he was a member of the Faculty of Electrical and Electronics Engineering, Bilkent University, Ankara, Turkey. In 2001, he joined the Faculty of Electrical and Electronics Engineering, Koç University, Istanbul, Turkey, as a Professor, and was the Dean of the College of Engineering from 2004 to 2009. Since September 2009, he has been the Vice President for Research and Development, Koç University. His recent research interests include numerical methods for electromagnetics and optics, printed circuits and antennas, and nanophotonics.

Krzysztof A. Michalski (S'78–M'81–SM'88–F'01) received the M.Sc. degree from the Technical University of Wroclaw, Wroclaw, Poland, in 1974, and the Ph.D. degree from the University of Kentucky, Lexington, in 1981, both in electrical engineering.

From 1982 to 1986, he was with the University of Mississippi. Since 1987, he has been with Texas A&M University, College Station. His primary research interest is in computational electromagnetics with an emphasis on Green's function-integral equation methods for objects in layered media.